Project Course Final

Craig Offutt

August 4, 2023

Abstract

This paper explores and summarizes three dissertations authored by Dr. Eric Farenthold's Ph.D. students, focusing on the Non-Holonomic Hamiltonian Method for engineering simulations. The primary objective of the course was to gain a comprehensive understanding of this method and its applications in engineering simulations, particularly in the context of shock physics.

The core emphasis of these dissertations lies in the development of multi-scale modeling techniques that combine computational and analytical approaches. Specifically, they employ finite element analysis (FEA) and Hamiltonian physics to create comprehensive and robust models. These modeling methods are instrumental in advancing our understanding of shock physics and find relevance in various engineering scenarios.

Chapter 1

Sangyup Lee's "Nonholonomic Hamiltonian Method for Multiscale Simulation of Reacting Shock Physics "

1.1 Introduction

The Nonholonomic Hamilton Method developed through the application of Hamiltonian Physics combined with finite element analysis, offers a novel system for solving problems and conducting simulations without relying on partial differential equations. Multiscale modeling, a modeling approach that incorporates multiple models operating at different scales, serves as a means to comprehensively describe complex systems. This approach becomes necessary when macroscale models lack accuracy, while microscale models suffer from inefficiency or an overwhelming amount of information. By integrating diverse perspectives, a reasonable compromise can be achieved between accuracy and efficiency. In his dissertation, Sangyup Lee aims to leverage the Nonholonomic Hamilton Method in the field of shock physics, specifically for detention simulation, by employing a multiscale modeling framework.

1.2 Methodology

The majority of the three chapters, along with the initial part of Chapter 4, are dedicated to the comprehensive exploration of the dissertation's methodology. Each subsection will break down the methods employed. The objective of this section is to present a comprehensive overview of the dissertation's explanation for the multi-scale modeling of reacting shock physics.

1.2.1 Introduction (Chapter 1)

Chapter 1 sets the stage by introducing the topic of multiscale reacting shock physics simulation. It emphasizes the need for a systematic approach to integrating different numerical methods developed for different scales to effectively address the multiscale multiphysics simulation problem. The chapter discusses the various numerical methods used in computational research on reacting shock physics simulation, including macroscale continuum hydrocodes, mesoscale discrete or finite element formulations, and molecular dynamics models. It points out the limitations of current computational research, which often relies on empirical descriptions to address the wide range of spatiotemporal scales involved in shock-to-detonation simulations. The chapter proposes a modeling approach that combines fundamental balance laws with molecular-scale chemistry to develop a multiphysics model, reducing the reliance on empirical formulations.

1.2.2 Synchronous Multiscale Modeling Approach (Chapter 2)

Chapter 2 focuses on the synchronous multiscale approach to modeling reacting shock physics. It highlights the theoretical significance of this approach, even though it may limit the time scale addressable in practical simulations. The chapter describes the kinematics and structure of the multiscale model. At all scales, the numerical formulation is Lagrangian, but the kinematics vary. Particles are used at the molecular scale, finite elements at the mesoscale, and hybrid particle-element kinematics at the macroscale. Nonholonomic constraints link the three scales, allowing for seamless transitions between them. The hybrid particle-element kinematics employed at the macroscale enables the simulation of shock-induced fracture, fragmentation, and melting processes. The chapter explains the advantages of the developed multiscale formulation, such as admitting general nonlinear effects, incorporating electronegativity equilibration calculations, and conserving energy. Future research opportunities, including extending the formulation to additional energy domains, scales, and reference frames, are also mentioned.

1.2.3 Asynchronous Multiscale Modeling Approach (Chapter 3)

Chapter 3 introduces an asynchronous multiscale approach for simulating reacting shock physics. Previous research has utilized various techniques at different scales, such as continuum finite element, mesoscale particle, and molecular dynamics methods. However, merging these methods has been challenging due to differences in model formulation techniques used at different scales. The chapter presents a unified formulation that employs a discrete nonholonomic Hamiltonian method at all scales. The formulation combines Eulerian and Lagrangian frames, as well as a combination of finite element, particle, and hybrid particle-element kinematics. Geometric and material nonlinearities are considered in the formulation as well. The chapter provides example simulations to demonstrate the application of the meso-macroscale models in the context of explosives modeling. The mesoscale simulations focus on modeling thermomechanical wall shocks in an inert medium with voids, aiming to predict "hot spots" that may lead to explosive ignition. The macroscale simulations involve modeling thermomechanical and reacting thermomechanical wall shocks, aiming to predict shock-induced detonation and explosive propagation. The hybrid particle-element method employed in the simulations eliminates the need for legacy contact-impact modeling methods, making the approach more efficient. Mixture theory is used to simulate the thermodynamics of the reactive materials. The chapter also includes validation simulations that show good agreement with exact solutions and experimental data.

1.2.4 Incorporation of Chemistry Models and Equations of State (Chapter 4)

Chapter 4 delves into the integration of chemistry models and equations of state in multiscale simulations. The chapter explains that detailed molecular dynamics simulations are performed to understand the reaction mechanisms and kinetics of the reactive materials at the molecular scale. From these simulations, simplified reaction mechanisms and kinetics models are derived. The equation of state for the explosive product intermediates is also determined. These molecular-scale models are then incorporated into the mesoscale and macroscale simulations. The chapter emphasizes the goal of replacing empirical models with a connected detonation chemistry model, which would enable the development of improved energetic materials. It highlights the critical tasks for successful implementation, such as effectively using the information from reacting molecular dynamics simulations and developing accurate equation of state models for the reactive materials.

1.3 Formulation

This section will delve into the formulation of both synchronous and asynchronous methods for multiscale modeling, as explored in Chapters 2 to 4 of the dissertation. A more extensive analysis will focus on the asynchronous approach due to its practicality and simulation testing. The formulation of the synchronous model will be discussed in Section 1.3.1. Subsequent sections, namely 1.3.2 through 1.3.3, will address the asynchronous model, beginning with the formulation of the mesoscale and macro-scale (Chapter 3). Next, the implementation of the molecular scale will be examined (Chapter 4).

1.3.1 Synchronous Multi-scale Modeling Approach (Chapter 2)

The modeling approach described in Chapter 2 provides a framework for understanding systems at multiple scales. It consists of three levels: macroscale, mesoscale, and molecular scale models. Each level focuses on different aspects of the system and contributes to a comprehensive understanding of its behavior.

At the macroscale level, the system is described using a Hamiltonian that combines kinetic energy and potential energy . The particles in the system are approximated as ellipsoids, and variables such as particle masses , center of mass positions , angular velocities, and inertia tensors are considered. The particle densities are computed using rate equations that take into account neighboring particles and their interaction ranges. The evolution equations for internal energy consider molecular, mesoscale, and macroscale terms, accounting for factors like pressure and fragmentation. Nonholonomic constraints link the different scales, and the Hamilton's equations govern the dynamics of the system.

Moving to the mesoscale model, it represents a unit cell within a macroscale element using large strain Lagrangian finite elements. The Hamiltonian for a generic unit cell includes kinetic energy and potential energy . The deformation of the unit cell is influenced by the macroscale rate of deformation tensor. The focus of the mesoscale model is on the deformation of the unit cell rather than rigid body translation or rotation. The internal energies are governed by elastic strain energy and irreversible entropy production terms. Constitutive relations relate stress tensors to strain tensors and plastic strain . The mesoscale Hamilton's equations describe the dynamics of the unit cell.

At the molecular scale, it represents the particles within the hybrid particle element macro-scale frame. The system is described using a nonholonomic formulation of reacting molecular dynamics. The Hamiltonian includes kinetic energy and potential energy . The potential energy is computed by integrating various effects such as chemical bonds, Coulomb interactions, van der Waals forces, and external loading. This formulation allows for energy-conserving bond breaking and forming and accounts for nonlinear effects. The potentials are morphing potentials that depend on the positions and velocities of the particles.

The macroscale model captures the overall dynamics and interactions, while the mesoscale and molecular scale models delve into finer details at their respective levels. This multi-scale perspective provides a comprehensive understanding of the system's behavior and enables the analysis of complex phenomena. Below is Figure 2.1 from Dr.Lee's dissertation describing the relationship between each level of the system.

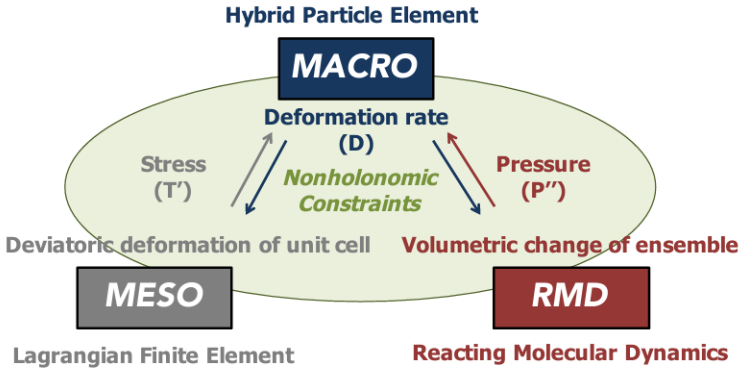

Figure 2.1: Structure of the synchronous multiscale model

1.3.2 Asynchronous Multiscale Modeling Approach (Chapter 3)

Section 3 focuses on the Hamiltonian formulation in a one-dimensional setting and highlights its applicability to modeling systems at different scales. The formulation is based on fundamental Hamiltonian modeling concepts and extends previous work on Hamiltonian formulations for shock physics applications.

At the macroscale level, the model employs Eulerian finite elements to discretize the system. The macroscale Hamiltonian combines the kinetic energy term and the potential energy term. The kinetic energy term involves the momentum vector and the mass matrix, where the nodal velocities are related to the momentum vector. The potential energy term includes the element's internal energies , which serve as state variables. The macroscale Hamiltonian captures the dynamics of the system by considering the interactions between momentum, velocities, and internal energies.

To obtain a system-level model, the macroscale Hamiltonian is combined with the canonical Hamilton's equations, a virtual work expression, and nonholonomic constraints. The canonical Hamilton's equations describe the evolution of momentum, element internal energies, element masses, and species mass fractions with respect to their respective generalized nonconservative forces. The generalized nonconservative forces are determined by the virtual work and the nonholonomic constraints.

The virtual work expression, formulated in terms of quasi-coordinates, balances the rate of change of kinetic energy in the elements and at the nodes. It accounts for the work done by nonconservative forces and ensures energy conservation in the system. The nonholonomic constraints govern the evolution of the element internal energies and may include convection and irreversible entropy production terms. These constraints introduce additional generalized nonconservative forces that influence the dynamics of the system.

The degenerate Hamilton's equations associated with the nonholonomic constraints determine the Lagrange multipliers, which are used to enforce the constraints. By incorporating these equations and considering the Lagrange multipliers, the macroscale formulation is completed. The formulation allows for the modeling of various phenomena, such as large strain kinematics, chemical-thermomechanical coupling, plastic compaction of voids, mixed solid-gas thermodynamics, and nonuniform void distributions.

At the mesoscale level, the Hamiltonian formulation follows a similar functional form as the macroscale case but with some modifications. The model represents a unit cell of one Eulerian finite element and employs a Lagrangian hybrid particle-finite element array. The mesoscale Hamiltonian considers a diagonal mass matrix with particle masses along the diagonal and relates the particle velocities to the momentum vector through the equation. The Lagrangian particles are located at the finite element nodes, and the elements quantify the large strain Lagrangian forces associated with tension and shear.

The canonical mesoscale Hamilton's equations describe the dynamics of particle momenta , positions , and internal energies . Similar to the macroscale formulation, these equations incorporate generalized nonconservative forces and nonholonomic constraints. The nonholonomic constraints at the mesoscale include terms such as mechanical power and irreversible entropy production, which affect the evolution of particle internal energies.

The degenerate Hamilton's equations associated with the internal energies determine the Lagrange multipliers that enforce the nonholonomic constraints. Additionally, a virtual work expression is introduced to account for external loads in the mesoscale formulation. The overall dynamics of the system, including the positions, internal energies, and momenta of the particles, are represented in an explicit state space form.

The mesoscale formulation is particularly suitable for modeling fracture and fragmentation, as it incorporates true Lagrangian modeling in these processes. The method uses singular interpolation kernels and avoids particle streaming. It has been successfully applied to model shock physics problems at high velocities, such as orbital debris impacts.

One notable aspect of the Hamiltonian formulation is its ability to handle non-continuum effects, such as fracture and fragmentation, without explicitly relying on partial differential equations. This feature provides flexibility in modeling various physical phenomena and allows for the incorporation of complex behaviors at different scales. The formulation also offers a solid foundation for further development and expansion, enabling the introduction of additional energy domains or scales to enhance the modeling capabilities.

Below is Figure 3.1. It displays the structure of the meso-macroscale model

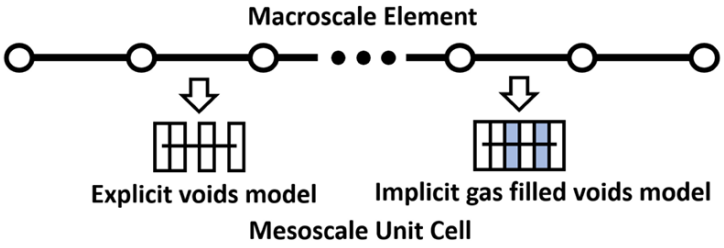

Figure 3.1: Structure of the meso-macroscale model.

1.3.3 Incorporation of Chemistry Models and Equations of State (Chapter 4)

Chapter 4 discusses the integration of molecules into the previously derived model from Chapter 3 to create an engineering model of the detonation process. The integration aims to replace empirical detonation modeling components with models directly connected to detonation chemistry, thereby improving the application of accumulated knowledge to enhance the design and understanding of energetic materials.

The suggested integration approach involves multiple steps. Initially, reacting molecular dynamics simulations are used to determine simplified initial and final reaction mechanisms, as well as associated kinetics models, that describe the decomposition of the explosive and the formation of explosive product intermediates. These simulations provide valuable insights into the chemical processes occurring at the molecular level.

Equations of state for the explosive product intermediates are then determined using reacting molecular dynamics simulations. This involves either tabulation or fitting coefficients to an analytic equation of state. The equations of state provide information about the thermodynamic properties of the intermediate products, which is crucial for modeling their behavior.

Mesoscale simulations are performed next, incorporating the short-time kinetics model and the equation of state for the explosive product intermediates. These simulations aim to develop an internal state variable model that relates local conditions at hot spots to macroscale thermodynamic states. The model quantifies the time delay associated with hot spot development, which is important for understanding the detonation process.

Finally, macroscale simulations are conducted, incorporating the long-time kinetics model and the internal state variable model of hot spot conditions. These simulations are used to model shock to detonation, providing insights into the overall behavior of the detonation process.

The integration approach presented in Chapter 4 replaces empirical detonation modeling components with models directly connected to detonation chemistry. This enables the application of accumulated knowledge in detonation chemistry to improve the understanding and design of energetic materials. The approach involves the development of chemical kinetics models, an ignition process model, equations of state, and state interpolation techniques.

The short-time chemistry model describes the decomposition of solid explosives and the generation of intermediate reaction products. The long-time chemistry model focuses on the transition from intermediate reaction products to long-term products observed in experiments. The ignition process model, obtained from mesoscale simulations, describes the initiation and growth of the detonation. State interpolation techniques are used to determine composite equations of state at different scales.

By utilizing reacting molecular dynamics simulations and incorporating chemistry models directly connected to detonation chemistry, the integration approach aims to overcome the limitations of empirical models and improve the accuracy and predictive capabilities of detonation simulations. It also enables the consideration of complex phenomena and provides a foundation for further advancements in the field of energetic materials. Below are figures 4.1 and 4.2 which show the visualization of how the molecular scale is implemented into the meso-macroscale.

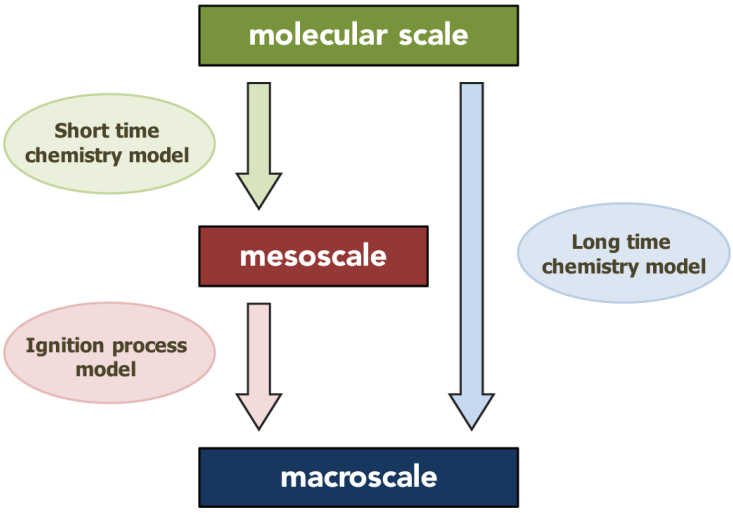

Figure 4.1: Asynchronous mutiscale integration strategy.

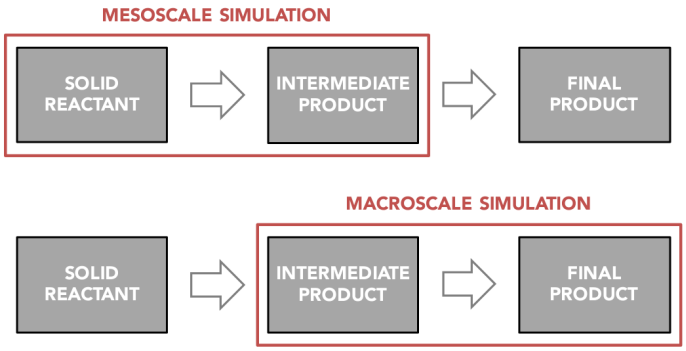

Figure 4.2: Functions of the short time chemistry model [6] (upper figure) and long time chemistry model [6] (lower figure).

1.4 Numerical Implementation and Validation

The numerical implementation, as well as the veracity of the formulation and simulation, have been subjected to empirical scrutiny. These aspects are thoroughly examined in Chapters 5-7 of the dissertation. Section 1.4.1 comprehensively addresses the implementation and establishes the model's validity at the individual scale, specifically focusing on the flyer plate impact test problem with TNT and Composition B as the explosive. Section 1.4.2 delves into the implementation and assesses the validity of the complete asynchronous multi-scale model formulated in Chapters 3-4.

1.4.1 Validation of the Individual Scales (Chapter 5)

The simulations focus on modeling shock to detonation for flyer plate impacts at different velocities in TNT and Composition B explosives. The models employ the Jones-Wilkins-Lee (JWL) equations of state for the solid reactant and gas product, as well as an ignition and growth model for the explosive.

Below is Figure 5.6 which demonstrates the convergence of the mesoscale models' simulations by comparing the predicted detonation velocities with the corresponding experimental velocities as a function of model resolution for both TNT and Composition B.

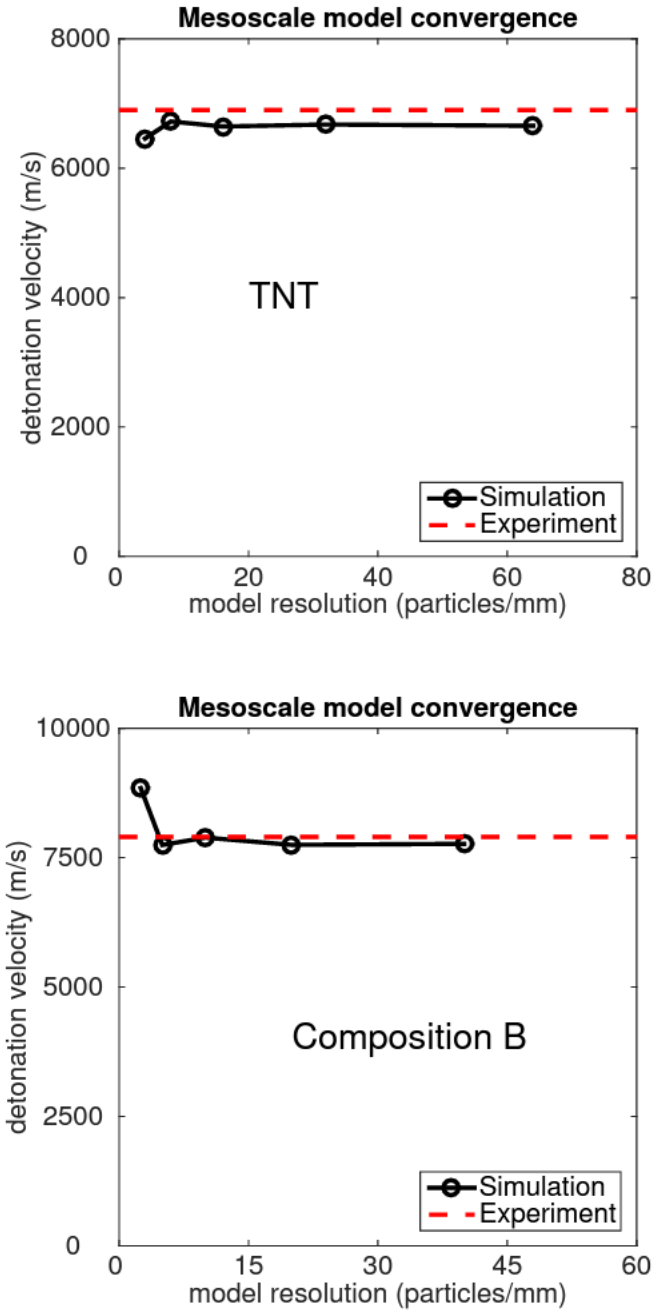

Figure 5.6: Mesoscale simulations: convergence test results for TNT (upper figure) and Composition B (lower figure).

1.4.2 Simulation of Detonation using HMX and RDX (Chapter 6 and Chapter 7)

Mesoscale Implementation (Chapter 6.1)

The implementation of the mesoscale simulation of HMX and RDX involves integrating a short-time chemistry model with a mesoscale hotspot generation model. The mesoscale formulation employs a Lagrangian hybrid particle-element array and discrete Hamilton's equations to model the system. It extends previous work by incorporating chemistry models and reaction dynamics into particle-element

discretization. Additional nonholonomic constraints are introduced for species concentration evolution equations, and Lagrange multipliers are used to determine the nonconservative generalized forces for species concentrations.

The mesoscale formulation also incorporates new equations of state that depend on reaction progress variables. A solid reactant equation of state and a detonation products equation of state are used to complete the global model. The specific equations of state are taken from the literature. The chemical kinetics model used in the simulation is a simplified 4-step short-time (detonation) chemistry model. The model includes reaction rates and species concentration evolution equations for various species involved in chemical reactions.

Simulation results are obtained by integrating the ordinary differential equations using a Runge-Kutta second-order method. Below is Figure 6.16 and Figure 7.15 which demonstrates the convergence of the mesoscale models' simulations by comparing the predicted detonation velocities with the corresponding experimental velocities as a function of model resolution for HMX and RDX respectively.

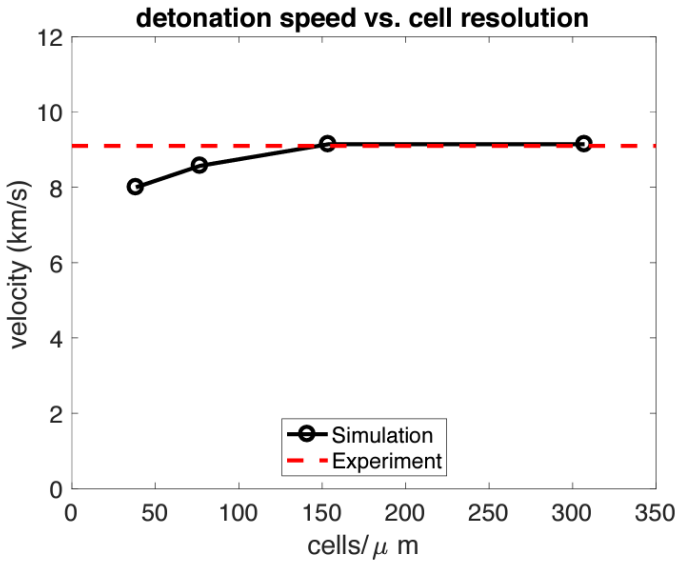

Figure 6.16: Convergence test: mesoscale simulation in HMX.

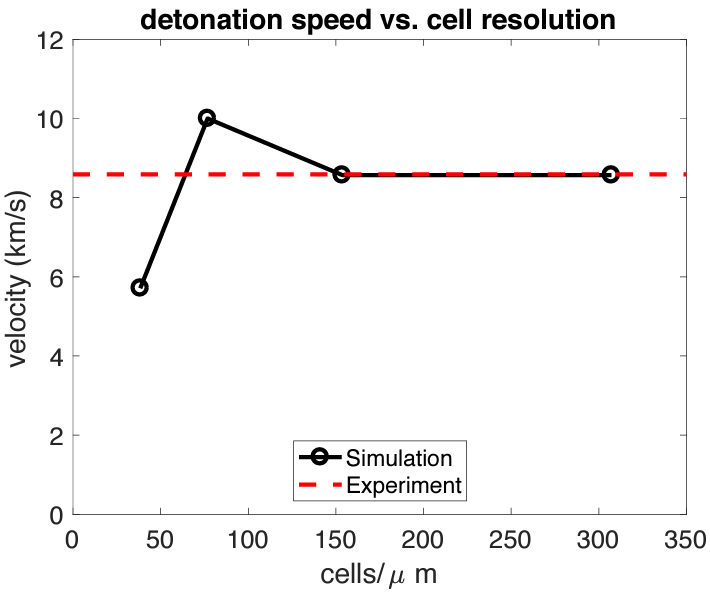

Figure 7.15: Convergence test: mesoscale simulation in RDX.

Macroscale Implementation (Chapter 6.2)

The macroscale model is based on an Eulerian finite element array and utilizes discrete Hamilton's equations that incorporate chemical kinetics for a reacting system. The equations of state are developed to express pressure and temperature as functions of various variables such as element masses, internal energies, ignition process variables, macroscale reaction progress variables, and species concentrations.

The model considers the discretization and constitutive relations using finite element interpolation and a system-level model. The evolution of mass and internal energy conservation is described using conservation equations from previous work. The mass conservation equations depend on a coefficient matrix that is a function of element masses. The internal energy evolution equations consider convection, mechanical power flow, dissipated power, and heat conduction power flow.

An ignition process model is introduced to describe the evolution of detonated masses. The model includes convection of the reacted masses and an ignition source term. The convected term depends on interface density, interface reacted mass, interface mass, and interface material velocity. The source terms consider factors such as detonation velocity, characteristic length, and a pressure-dependent ignition criterion.

The evolution of species masses is determined by the convection of species masses and reaction source terms. A homologous temperature variable is introduced to map molecular scale to macroscale temperatures. The species mass conservation equations involve partial derivatives, reference species mass fractions, and reacting MD simulation results.

Nonholonomic constraints are implemented using backward difference approximation. The pressure and temperature evolution equations are derived, considering the dependencies on internal energy, mass, and species. The species mass evolution equation is obtained by substituting the derived pressure and temperature evolution equations into the species mass conservation equation.

Overall, the implementation of the macroscale simulation model involves formulating the equations of state, describing the discretization and constitutive relations, conserving mass and internal energy, modeling the ignition process, evolving species masses, and imposing nonholonomic constraints.

The simulation employed a fourth-order Runge-Kutta method for integrating the ordinary differential equation (ODE) model. Below is Figure 6.29 and figure 7.27 which demonstrates the convergence of the mesoscale models' simulations by comparing the predicted detonation velocities with the corresponding experimental velocities as a function of model resolution for HMX and RDX respectively.

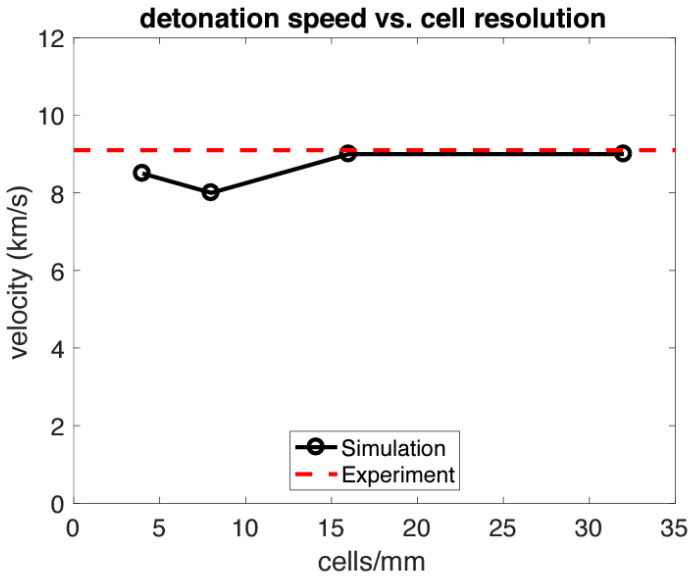

Figure 6.29: Convergence test: macroscale simulation in HMX.

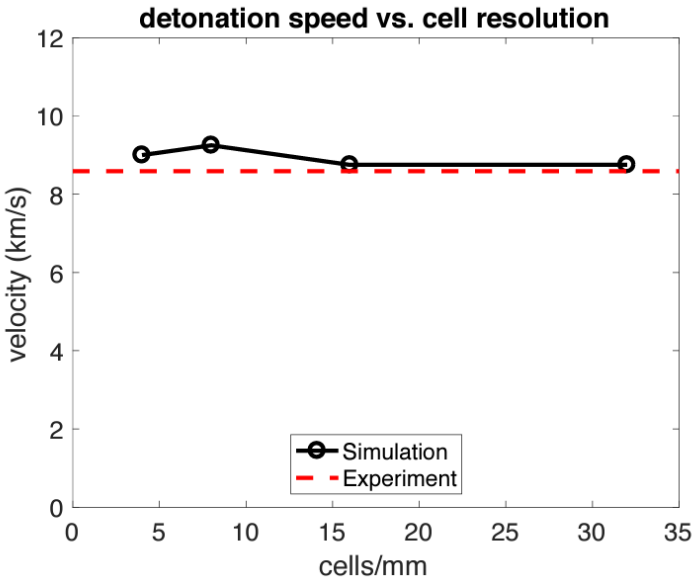

Figure 7.27: Convergence test: macroscale simulation in RDX.

1.5 Conclusion

Sangyup Lee's report focuses on enhancing detonation simulations by employing a multi-scale approach to simulate reacting shock physics. The report discusses both synchronous and asynchronous modeling techniques, addresses the integration of chemistry models, and explores the incorporation of equations of state. His paper addresses the limitations of empirical models and offers insights and predictive capabilities in detonation simulations.

Chapter 2

Joseph Bass's "Nonholonomic Hamiltonian Method for Reacting Molecular Dynamics (RMD) "

2.1 Introduction

The development of explosives in both commercial and defense applications has traditionally relied on experimentation. Modern explosive compositions mainly utilize energetic materials that have been available in their basic form for at least fifty years; however, recent research in explosives has focused on two main themes.

The first theme involves the development of new energetic materials with reduced sensitivity. This is crucial in order to enhance safety in handling and storage. The second theme centers around the increased use of computation as a complement to experimentation. Computational methods are employed to aid in the development of new energetic materials that possess reduced sensitivity and improved performance.

The significance of insensitive munitions in defense applications is widely acknowledged due to past accidents that highlight the potential hazards involved. Notable incidents include accidents at Thule, Greenland, on board the USS Forrestal, and at Camp Doha, Kuwait. The challenges inherent in conducting high-speed, high-pressure, and high-temperature experiments, coupled with advancements in computing capabilities, have prompted researchers to explore the potential of modeling and simulation in the design of energetic materials.

Various models, such as macroscale, mesoscale, and ab initio models, are employed to study reacting shock physics. These models are generally based on rate law descriptions of the chemical processes under investigation. At the macroscale level, rate laws are ordinary differential equations that describe the rates of change in reactant and product concentrations. On the other hand, at the ab initio level, the rate law of interest is the time-dependent Schrödinger equation, which is a partial differential equation that describes the evolution of the electronic wave function. Both types of rate laws explicitly account for transitions between equilibrium states. However, in molecular scale simulations, position-dependent potential functions are typically used to represent the physics of chemical reactions, deviating from the typical rate law descriptions.

Many people are aware of the difficulties in applying potential-based reactive molecular dynamics techniques to materials with intricate chemistry. An alternate molecular-scale modeling strategy has been devised to overcome this problem. It is important to note that rate laws, which define the kinetics of the bonding-debonding process, provide the basis for computational chemistry models utilized at greater (macro) and lower (electronic structure) scales. These formulations, known as Nonholonomic Hamiltonian Method (NHM), offer versatility in the modeling of nonlinear systems.

This paper will discuss the methodology, formulation, and simulation/validation of reacting molecular dynamics using the NHM from Joseph Bass's dissertation. It will be divided up into two sections. The first section will be the microcanonical ensemble or NVE Ensemble. The second section will discuss a model in which the system acts as an NVE Ensemble and then "converts" to a canonical or

NVD Ensemble.

2.2 NVE Emsemble

2.2.1 Methodology

This section introduces a new nonholonomic formulation of reacting molecular dynamics specifically designed for modeling detonation dynamics in condensed-phase explosives. It should be noted that the model discussed in this chapter is limited to applications of an NVE ensemble, a system involving a constant number of particles, volume, and energy. The model's derivation is presented in a condensed form.

2.2.2 Forumulation

The potential energy of an atom is determined using a rate equation that considers three factors: reactive potential energy, van der Waals contribution, and molecular mechanics contribution.

The reactive potential energy is obtained by integrating a term based on the distance between atoms (interatomic distance) and its rate of change. The interatomic distance is calculated as the square of the difference between atomic positions, and its rate of change is determined by the dot product of the difference in positions and their respective rates of change.

The bond order between atoms is determined by the sum of two bond lengths, and its rate of change is influenced by the rate of change of the bond length and a function that depends on certain parameters.

Atomic interaction forces are computed using non-analytic pseudo-potentials, which are derived from the derivative of the potential energy with respect to the interatomic distance.

Bass also includes that existing potential functions can be incorporated into this framework. An example is provided for the van der Waals potential energy, which is expressed differently based on the range of the interatomic distance.

2.2.3 Simulation/Validation

1-D Problem

An example 1-D problem is the simulation of detonation in solid nitric oxide. The initial configuration consists of a repeating chain of N-O O-N unit cells. The detonation reaction studied in this research is 2NO $\rightarrow$ N2 + O2. Three simulations were conducted with initial velocities of 4, 6, and 8 km/s.

The potential energy evolution equations involve nonholonomic constraints and include bonded and unbonded potential energy functions. The parameters and equations for these functions are provided. A Lennard-Jones potential is used to represent a container wall.

Below is Figure 2.2 from Bass's dissertation comparing the simulations of different detonation wave velocities versus empirical data.

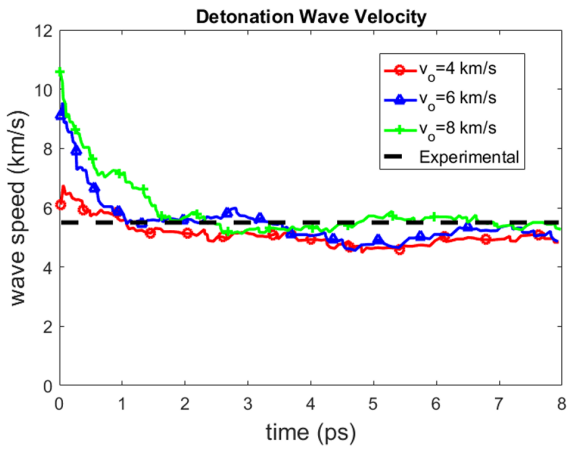

Figure 2.2: Wave velocity versus time for initial shocks of 4, 6, and 8 km/s (1-D example problem)

2-D Problem

A 2-D example problem is the detonation of a confined crystal composed of covalently bonded A-B molecules in a crystalline lattice. Previous research by NRL, ARL, and LANL is discussed, highlighting the use of exponential potentials with varying interpolation schemes. The section introduces a new RMD method for simulating the problem and provides an initial atomic configuration.

The numerical formulation includes evolution equations incorporating nonholonomic constraints and different potentials (repulsive, attractive-repulsive, and van der Waals). The potentials are expressed using exponential pseudo-potentials, similar to a reference paper but without certain components. Simulation results depict the progression of the detonation wave and report a computed detonation velocity of 10.2 km/s. Although there are no experimental data for comparison, previous studies have reported computed detonation velocities ranging from 6.6 km/s to 9.5 km/s. The obtained results align closely with recent work by LANL.

2.3 NVE with NVT Ensemble

2.3.1 Methodology

This section presents a formulation for simulating reacting shocks in the NVE (constant particle number, volume, and energy) and NVT (constant particle number, volume, and temperature) ensembles.

Experimental methods such as shock tube experiments, bomb calorimetry, pyrolysis, and spectroscopy have been used to investigate reaction mechanisms, rates, and decomposition products in energetic materials. However, measuring detonation dynamics experimentally remains challenging, leading to the need for complementary modeling research. Computational work using ab initio, molecular dynamics, and multiscale modeling methods has shown the value of coordinated experimental and computational research but has also highlighted the need for improved numerical models of detonation processes.

At the molecular scale, accurately simulating shock-induced detonation in condensed-phase explosives has been a prominent goal of computational research. This includes validating the numerical model against experimental data on energy release and detonation products, as well as predicting reaction mechanisms and rates under conditions that are difficult to measure experimentally. However, extending reacting potential methods developed over several decades to material systems with complex chemistry has been a significant challenge.

The detonation phenomena of interest are modeled in two phases. The first phase is an adiabatic disassociation phase, where the energetic material detonates under NVE conditions. In the second phase, the system is thermostatted to a designated temperature, leading to recombination.

2.3.2 Forumulation

Numerical Formulation

The kinetic energy is the sum of the translational kinetic energies of each atom, while the potential energy includes contributions from a wall potential and repulsive interactions. Each atom is treated as a point mass, so there is no rotational kinetic energy.

The wall potential models the repulsive interaction between atoms and the boundaries of the ensemble. It is defined by equations that depend on atomic positions and constants. The potential energy due to unbounded interactions is calculated using an interatomic potential function, which depends on the distance between atoms and empirical constants.

The formulation also describes the evolution equations for bond order and entropy. The bond order evolution equations determine the bonded states in the ensemble using a rate law. Empirical parameters such as effective valence matrices, bond type probability matrices, and bond cutoff distances are used in these equations. The bond order is computed based on the bond state variable, which is influenced by proximity and current bond state.

The text further explains the computation of bonding weights, estimation of bond order, and determination of new bonds based on random numbers assigned to atoms. The bond state variable and bond type are used to compute the right-hand side term in the evolution equations.

Finally, an over coordination check is performed to ensure that no atom exceeds its allowable number of bonds.

The text discusses the evolution of ensemble entropy in a physical system. It introduces three components that contribute to the entropy flow: bonding-debonding, viscous dissipation, and imposed conduction entropy flow.

The entropy flow due to bonding-debonding is influenced by the temperature and bonding forces between atoms. The attractive-repulsive force between bonded atoms and the repulsive force between unbonded atoms are described. The entropy flow is inversely proportional to the ensemble kinetic temperature.

Viscous dissipation leads to irreversible entropy generation in the system. It is influenced by a global force vector obtained from a damping coefficient and applied within a specific time range. The entropy flow due to viscous effects is also inversely proportional to the ensemble kinetic temperature.

An imposed conduction entropy flow is used to control the ensemble kinetic temperature. It has a functional form that adjusts the entropy flow rate based on the desired system temperature.

The power input and output of the system are determined by the imposed conduction entropy flow. The net power flow into the system is influenced by the entropy flow, bonding-debonding forces, and viscous forces.

The text also mentions the canonical Hamilton's equations, which describe the dynamics of the system. It introduces generalized forces, including conservative forces derived from the potential energy and nonconservative forces associated with the net power flow. Lagrange multipliers are introduced to incorporate nonholonomic constraints related to bond order and entropy evolution.

Finally, Hamilton's equations are presented, which govern the evolution of the system. These equations consider the forces, including bonding forces, entropy flow, and nonconservative forces. The integration of the state space model is performed using Runge-Kutta with a time step of .01 femtoseconds.

Chemical Kinetics

Simulating shock-induced detonation at the molecular scale in condensed-phase explosives is a challenging task due to complex chemistry. The formulation considers kinetic and potential energies, including repulsive interactions and boundary effects. It describes bond order and entropy evolution equations, determining bonded states using empirical parameters. The entropy flow is influenced by temperature, bonding forces, and viscous dissipation, and an imposed conduction entropy flow controls the ensemble temperature. The power input and output depend on these factors. Canonical Hamilton's equations capture system dynamics, incorporating conservative and nonconservative forces with Lagrange multipliers for nonholonomic constraints.

This formulation addresses the need for simulating reacting shocks in the NVE and NVT ensembles to study detonation dynamics. It accounts for complex chemistry in condensed-phase explosives and involves kinetic and potential energies, bond order and entropy evolution equations, and canonical

Hamilton's equations. The entropy flow, bonding forces, and viscous dissipation play key roles in the simulation, while the imposed conduction entropy flow controls the temperature.

2.3.3 Simulation and Validation

Alas, now it is time to look at the validation of the (RMD) formulation by simulating the detonation of HMX and RDX crystals and comparing the predicted results with experimental data. The simulations consist of two stages: the NVE stage, where the crystal is impacted and detonates, and the NVT stage, where the high-temperature intermediates recombine into the final detonation products. The simulation results are compared to experimental data for energy release and long-time detonation products. The reaction mechanisms and kinetic models for the detonation and recombination processes are obtained from the simulations. The simulations for HMX and RDX are described, including the initial setup, material-specific parameters, and crystal configurations.

Results for HMX

Below is Table 3.14 and 3.15 which illustrate the error in simulated energy release and simulated detonation products given a specific amount of molecules of HMX respectively.

Table 3.14: Error in the simulated energy release: HMX

	8 Molecules	16 Molecules	32 Molecules	64 Molecules
error	0.0249	0.0257	0.0578	0.0665

Table 3.15: Error in the simulated detonation products: HMX

	8 Molecules	16 Molecules	32 Molecules	64 Molecules
error	0.1217	0.1562	0.1406	0.0542

Next, Figure 3.9 illustrates the simulation temperature with respect to time for HMX.

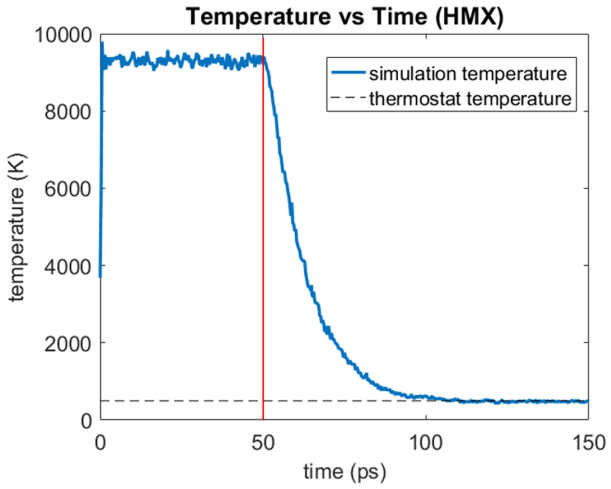

Figure 3.9: Temperature versus time (left of vertical line is NVE, right of vertical line is thermostatted): HMX

Results for RDX

Below is Table 3.37 and 3.38 which illustrate the error in simulated energy release and simulated detonation products given a specific amount of molecules of RDX respectively.

Table 3.37: Error in the simulated energy release: RDX

	8 Molecules	16 Molecules	32 Molecules	64 Molecules
error	0.0938	0.1236	0.1207	0.1285

Table 3.38: Error in the simulated detonation products: RDX

	8 Molecules	16 Molecules	32 Molecules	64 Molecules
error	0.2979	0.0949	0.1140	0.0946

Next, Figure 3.9 illustrates the simulation temperature with respect to time for RDX.

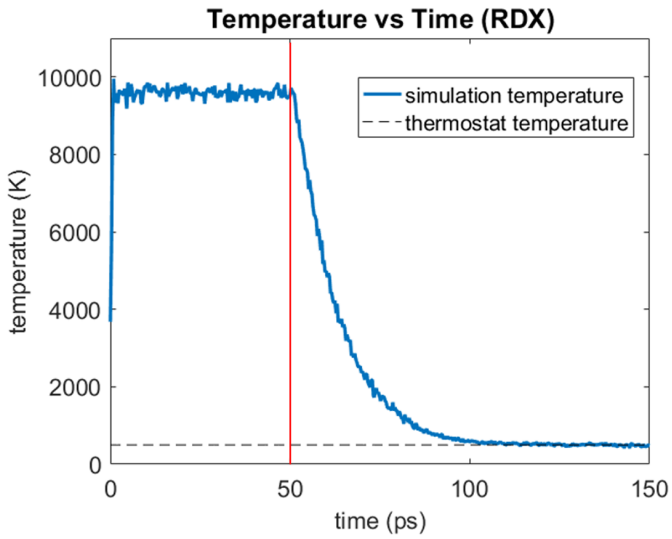

Figure 3.50: Temperature versus time (left of vertical line is NVE, right of vertical line is thermostatted): RDX

2.4 Conclusion

This paper explores the use of computational methods, specifically the Nonholonomic Hamiltonian Method (NHM), for simulating reacting molecular dynamics in the development and understanding of explosive materials. It addresses the challenges of reducing sensitivity and improving performance by complementing experimentation with computational approaches.

The NHM formulation in the NVE ensemble focuses on modeling detonation dynamics in condensed-phase explosives. It covers factors such as reactive potential energy, van der Waals contribution, molecular mechanics, and atomic interaction forces.

The NHM formulation to the NVT ensemble enables the simulation of reacting shocks and recombination processes. It includes kinetic and potential energies, entropy flow, bonding forces, and viscous dissipation, utilizing canonical Hamilton's equations to capture system dynamics.

Simulation and validation results for HMX and RDX crystals showcase the NHM's accuracy in predicting energy release, detonation products, and reaction mechanisms. The paper's findings contribute to the advancement of computational methods in explosives research and offer valuable insights into the behavior and performance of energetic materials.

Chapter 3

Jie Zhang's "Computational Design of Gas Phase Explosive Sensors"

3.1 Introduction

The dissertation focuses on the sensing performance of graphene-based explosive sensors, the development of a dual-mode sensing method for gas phase explosives, and the formulation of an adaptive ab initio molecular dynamics method. The research aims to advance the field of nanocomposite explosive sensing systems by using graphene as a foundation material. The dissertation investigates various sensor parameters, including sensor bases, doping effects, junction effects, bending effects, and a docking method for sensitive and selective sensor design.

The research background emphasizes the potential of nanocomposites in modifying material properties for explosive sensing. It discusses the limitations of existing explosive sensing technologies and highlights the advantages of graphene-based sensors, such as high strength, thermal conductivity, and electrical conductivity. Computation is identified as a valuable tool for accelerating experimental research and exploring new physical phenomena. The dissertation introduces a new ab initio molecular dynamics formulation that simulates multiphysics sensing transients and interaction with the thermal environment.

The research scope covers six engineering fields: computational materials design, chemiresistive sensing, nanocarbon conductance and junctions, electromechanical coupling in nanocarbons, and multimode sensing. Each field is briefly described, highlighting their interconnections and relevance to sensor design. This paper will cover the subsequent chapters and provide research on each field, including the formulation of the model and validation against experimental data.

3.2 Chapter 2: An Adaptive Ab Initio Molecular Dynamics Formulation for Material Design

3.2.1 Numerical Model

The section discusses a numerical model for nanocomposite explosive sensors. The model combines adaptive ab initio molecular dynamics with a macro-scale thermal environment. The system consists of nuclei and electrons, with the Hamiltonian expressed as the sum of kinetic and potential energies for nuclei and the total energy for electrons.

$$H = T_n + V_n + E_e$$

The nuclear kinetic co-energy, momenta, and potential energy are defined. The electronic energy includes electron repulsion, electron-nuclear attraction, and electron kinetic energy, computed from the electronic wave function. The wave function is interpolated using time-varying radii and wavenumbers. Evolution equations are introduced to describe the time variation of basis coefficients. The mixed classical-quantum system is coupled using a nonholonomic modeling approach. Canonical Hamilton's

equations are derived, including momentum balance equations.

$$\dot{\mathbf{p}} = -\frac{\partial H}{\partial \mathbf{q}} + \mathbf{f}^q, \quad \dot{\mathbf{q}} = \mathbf{M}^{-1}\mathbf{p}, \quad \mathbf{0} = -\frac{\partial H}{\partial \mathbf{a}} + \mathbf{f}^a, \quad \mathbf{0} = -\frac{\partial H}{\partial \mathbf{k}} + \mathbf{f}^k$$

$$\mathbf{0} = -\frac{\partial H}{\partial \mathbf{c}'} + \mathbf{f}', \quad \mathbf{0} = -\frac{\partial H}{\partial \mathbf{c}''} + \mathbf{f}''$$

Nonholonomic constraints, including the discrete Schrodinger equations and thermal dissipation, are incorporated using Lagrange multipliers. The final Hamilton's equations for the system are presented.

$$\dot{\mathbf{p}} = -\frac{\partial H}{\partial \mathbf{q}} - \hat{\mathbf{A}}^T \frac{\partial H}{\partial \mathbf{a}} - \hat{\mathbf{K}}^T \frac{\partial H}{\partial \mathbf{k}} - \mathbf{W}'^T \frac{\partial H}{\partial \mathbf{c}'} - \mathbf{W}''^T \frac{\partial H}{\partial \mathbf{c}''} - \frac{R}{2nk_B}\left(1 - \frac{\theta_e}{\theta}\right)\mathbf{p}$$

$$\dot{\mathbf{q}} = \mathbf{M}^{-1}\mathbf{p}$$

$$\dot{\mathbf{c}}' = \mathbf{W}'\mathbf{M}^{-1}\mathbf{p} + \mathbf{C}^{-1}\mathbf{D}\mathbf{c}, \quad \dot{\mathbf{c}}'' = \mathbf{W}''\mathbf{M}^{-1}\mathbf{p} + \mathbf{C}^{*-1}\mathbf{D}^*\mathbf{c}^*$$

$$\dot{\mathbf{a}} = \hat{\mathbf{A}}\mathbf{M}^{-1}\mathbf{p}, \quad \dot{\mathbf{k}} = \hat{\mathbf{K}}\mathbf{M}^{-1}\mathbf{p}$$

This numerical model provides an energy-conserving, multiscale, multiphysics approach for studying nanocomposite explosive sensors.

3.2.2 Validation

The section discusses the validation of the theoretical ab initio model developed in the dissertation. The validation work includes the parallel three-dimensional implementation of the electronic and nuclear scale models, the development of a numerical approach to reduce electronic structure time constants, and one-dimensional simulations of bonding in different molecules. The implementation assumes a screened Coulomb potential and weak long-range attraction forces. The approach avoids introducing fictitious electronic momentum states and provides an energy and charge-conserving adjustment of the electronic structure time constants. Table 2.1 show how simulations compare the computed bond lengths of seven molecules to experimental values.

Table 2.1: Experimental and computational bond lengths (Bohr)

Molecule	Bond	Experimental Bond Length	Computational Bond Length
H_2	H-H	1.3989	1.7861
C_2	C-C	2.3497	2.1878
N_2	N-N	2.0747	2.1637
O_2	O-O	2.1323	2.1937
CO	C-O	2.1323	2.2216
CO_2	C-O	2.1985	2.2304
HCN	H-C	2.0108	2.1518
HCN	C-N	2.1858	2.4763

Additionally, convergence tests and two-dimensional simulations are mentioned as ongoing or future work. The bond graph representation, shown below, used in this work is highlighted as a novel contribution.

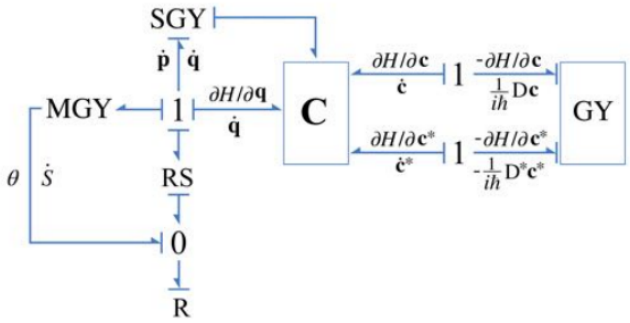

3.3 Chapter 3: Graphene Based Chemiresistive Sensing of Gas Phase Explosive

3.3.1 Modeling Approach

The development of lightweight, low-power sensors for gas phase explosives detection is challenging due to the low room temperature vapor pressures of many explosives. High sensitivity and selectivity are required for effective trace detection. Graphene and its derivatives offer promising candidates for miniature gas detectors due to their high specific surface area. This chapter discusses the development of ab initio models of graphene-based explosive sensors in different configurations to evaluate their performance in chemiresistive detection of commonly used explosive molecules (HMX, RDX, and TNT) and background gases (N2, O2, CO2, and H2O). The models quantify conductance changes in graphene platelets due to adsorbed gases, as well as adsorption energy and charge transfer. The configurations studied include pristine graphene platelets, functionalized platelets, and nanoholed platelets. Below are computational results for conductance and adsorption energy for various gas species.

Adsorbed species	Pristine surface	Pristine edge	C-O-C functionalized	C-OH functionalized	Nanohole patterned
conductance					
none	3.000	3.000	2.854	1.970	1.810
N_2	2.922	2.963	2.874	1.989	1.714
O_2	2.261	1.950	2.390	2.303	1.621
CO_2	2.917	2.832	2.894	1.943	1.721
H_2O	2.939	2.778	2.919	1.927	1.785
HMX	2.923	2.829	2.803	1.930	1.903
RDX	2.928	2.716	2.820	1.920	1.887
TNT	2.822	2.854	2.759	1.938	1.924
adsorption energy					
N_2	-0.089	-0.020	-0.429	-0.507	-0.320
O_2	-0.279	-0.233	-0.703	-1.249	-0.873
CO_2	-0.174	-0.089	-0.481	-0.570	-0.460
H_2O	-0.121	-0.181	-0.659	-0.773	-0.627
HMX	-1.267	-0.535	-1.982	-1.752	-1.586
RDX	-1.174	-0.891	-1.880	-1.880	-1.414
TNT	-1.596	-0.610	-1.343	-1.209	-1.006

3.3.2 Pristine GNR Sensors

This subsection discusses the sensing performance of pristine graphene nanoribbons (GNRs) as a basic material. Two sensing configurations, surface sensing, and edge sensing, are considered. Large-area monolayer graphene can be produced in mass with low cost, but it has a polycrystalline structure due to the fabrication process, which affects its sensing performance. Graphene platelets and single-crystalline GNRs are more suitable for computational sensor design. Atomically precise thin GNRs with widths less than ten nanometers have been fabricated using bottom-up methods.

Computational results are presented for the conductance change and adsorption energy of three different explosive molecules and four different background gases on both pristine GNR surface and edge sensing configurations. The results show that all target molecules reduce the GNR conductance. In the surface sensing configuration, O2 produces the largest change in conductance, while in the edge sensing configuration, all target molecules (except TNT and N2) show a larger change in conductance. The adsorption energies for explosive molecules are greater than those for background gases.

The conductance change mechanisms are analyzed for O2 and HMX adsorption on pristine graphene in both surface and edge sensing configurations. The charge transfer and HOMO-LUMO structure metrics are found to be strongly correlated with the computed conductance changes, while the density of states metric is not.

The results are consistent with some published experimental studies, and they suggest that large-area graphene is suitable for TNT sensing, while nanoribbon-based edge sensing is more suitable for nitramine explosives detection.

Overall, the study provides insights into the sensing capabilities of pristine GNRs and the factors affecting their performance when used as sensors for various target molecules.

3.3.3 Functionalized GNR Sensors

This subsection discusses the modeling results for graphene platelets with functional groups C-O-C and C-OH on their surface. Graphene oxide, decorated with epoxy (C-O-C) and hydroxyl (C-OH) functional groups, has been studied for various applications, including gas sensing. Computational results show that both functionalized models exhibit a reduction in conductance compared to pristine graphene, with the C-O-C groups being more stable and the C-OH groups more chemically active. The interaction between adsorbed molecules and the functional groups or graphene surface determines the conductance change direction.

In the case of C-O-C functionalization, O2 interacts more with the graphene surface, leading to reduced conductance, while CO2 and H2O interact more with the functional group, increasing conductance. For C-OH functionalization, O2 interacts strongly with the functional group, increasing conductance, while CO2 and H2O interact with the graphene surface, reducing conductance. The charge transfer, density of states, and HOMO-LUMO structure metrics correlate with the conductance changes in both functionalized cases.

The results align with published experimental studies on reduced graphene oxide sensors exposed to H2O and DNT. However, the complex response of functionalized sensors highlights the need for further modeling work to estimate overall sensor performance in the presence of gas mixtures, especially for explosive sensing applications.

3.3.4 Nanohole Patterned GNR Sensors

This subsection discusses modeling results for graphene platelets with a nanohole pattern, which has attracted attention for various applications, including gas sensing and selective identification of ions and molecules. Nanoholed graphene has shown improved sensing performance compared to regular graphene films. The computational results for a specific nanohole sensor configuration are presented, showing that conductance changes and adsorption energies vary depending on the target gases and background gases. Explosive molecules interact with numerous hole edge sites, leading to positive conductance changes, while background gases interact with only a few edge sites, resulting in negative conductance changes. The charge transfer mechanisms for O2 and HMX adsorption on nanoholed graphene are also discussed, indicating that the density of states changes are correlated with conductance changes, but other electronic properties show different behavior. However, the study acknowledges that more extensive computational work is needed to fully explore the effects of nanohole

patterning on graphene sensor performance.

3.4 Chapter 4: Doped Graphene Nanoribbons for High Specific Conductivity Wiring

3.4.1 Modeling Approach

This chapter describes a computational modeling procedure consisting of three steps to study how dopants affect the conductance of graphene nanoribbons (GNRs) and nanoribbon junctions. Here's a simplified summary:

The first step models how dopants affect the conductance of different types of GNRs: armchair GNRs with seven edges (7-aGNR) for semiconducting graphene, and zigzag GNRs with six edges (6-zGNR) for metallic graphene.

The second step focuses on modeling the impact of these dopants on the conductance of nanoribbon junctions. Different spatial distributions of dopants are considered, but this analysis is limited to 6-zGNR.

The third step combines the results from the nanoribbon and junction modeling with existing data on mean free path to create a nanowire model that can estimate the performance of larger conductors.

In the first two steps, calculations are done using periodic models in one direction, and a vacuum space is included in the other directions to avoid interactions with neighboring structures. Junction models are created by relaxing and adjusting the overlap of GNRs.

3.4.2 Doped Nanoribbon Model

Four configurations of potassium-doped GNRs are considered, including both semiconducting and metallic GNRs, with doping densities of one dopant atom per two unit cells (1/2) and one dopant atom per three unit cells (1/3). The distribution of potassium atoms along the GNR centerline is found to be stable, with the highest doping density being one atom per two unit cells. The transmission plots show that doping increases the conductance of semiconducting GNRs, with low-density doping (1/3) resulting in conductance values of G0 and high-density doping (1/2) further increasing the conductance to 2G0. In metallic GNRs, doping affects the Fermi energy conductance, with low-density doping maintaining the peak conductance and high-density doping increasing the Fermi energy conductance from G0 to 2G0. The DOS plots illustrate a left shift in the transmission distributions, indicating n-type doping for potassium-doped GNRs. The potassium atoms act as electron donors and establish low scattering pathways for charge carriers. The conductance change mechanisms are further analyzed using density of states (DOS) and charge density difference plots, which show a shift in the DOS distributions towards lower energies near the Fermi level. The potassium dopants effectively contribute to the DOS at the Fermi energy in the case of zigzag GNRs at the highest doping concentration. In summary, potassium doping transforms semiconducting armchair GNRs into metallic GNRs, increases the DOS near the Fermi level, and establishes low scattering pathways for charge carriers.

Similarly, four configurations of iodine-doped GNRs are modeled, with the same doping densities as potassium-doped GNRs. Iodine doping results in p-type doping for both armchair and zigzag GNRs. In armchair GNRs, doping at a density of 1/3 transforms them from semiconducting to metallic, while further increasing the doping density to 1/2 does not improve the Fermi energy conductance. In zigzag GNRs, iodine doping at a density of 1/3 increases the peak transmission value at the Fermi energy, but increasing the doping density to 1/2 reduces the transmission to match that of undoped GNRs, possibly due to the formation of triiodide. The DOS plots show a right shift in the DOS distributions, indicating p-type doping for iodine-doped GNRs. The charge density difference plots reveal that iodine dopants act as electron acceptors and establish low scattering pathways for charge carriers. The mass-specific benefits of iodine doping are more significant at the lower doping density. In summary, iodine doping transforms semiconducting armchair GNRs into metallic GNRs, increases the DOS near the Fermi level, and establishes low scattering pathways for charge carriers.

Overall, the results demonstrate the electrical properties and doping effects of potassium-doped and iodine-doped GNRs, providing insights into their conductivity and potential applications in electronic devices.

3.4.3 Doped Nanoribbon Junction Model

The section focuses on macroscale wiring, which requires the fabrication of GNR components. The conductance of undoped GNR junctions has been previously investigated and found to have periodic variations with a period of 18 unit cells for bilayer graphene and 7 unit cells for 7-aGNR.

The study examines different doping configurations, including potassium and iodine doping, with "internal" and "external" dopant atom distributions, as well as 1/3 and 1/2 doping densities. The dopant atoms are initially positioned above the center of a carbon hexagon. The conductance calculations for potassium-doped junctions show that internal doping extends the period of conductance variation and reduces its amplitude compared to undoped cases. This effect may be attributed to an increase in the separation distance between GNR layers, which impedes inter-ribbon electron transfer. In the internal doping configuration, there is no significant change in average junction performance when increasing the doping density from 1/3 to 1/2.

On the other hand, external doping improves junction conductance compared to internal doping, and the conductance level stabilizes based on the doping density. At larger overlaps, the conductances at high and low doping densities vary by approximately a factor of two. The external doping configuration minimizes the separation distance between GNR layers, resulting in enhanced conductance. Density of states (DOS) plots indicate that the dopant atoms (potassium or iodine) contribute significantly to the DOS near and above the Fermi level.

For iodine-doped junctions, the conductance variations are also affected by the doping density and configuration. In the internal doping configuration, increasing the doping density appears to reduce the junction conductance at high overlaps. In the external doping configuration, the junction conductance at high overlaps stabilizes independently of the doping density. DOS plots show that iodine atoms contribute significantly to the DOS at the Fermi energy.

In summary, the study demonstrates that doping affects the conductance of GNR junctions. Doping reduces the amplitude and extends the period of conductance variations with GNR overlap. Internal doping decreases the average junction conductance due to increased separation between GNR layers, while external doping improves conductance by minimizing the separation distance. Increasing the doping density generally enhances conductance, particularly in the case of potassium doping. However, increasing the iodine doping density from 1/3 to 1/2 does not lead to an improvement in average conductance.

3.4.4 Nanowire Model

This subsection discusses the construction of a macroscale model for doped graphene nanoribbon (GNR) conductors and their performance estimation. The model requires transmission properties obtained from ballistic conductance calculations and inputs such as a geometry model for the nanowires and scaling information. The nanowire model consists of overlapped nanoribbons, and its specific conductivity is determined by the length of the segment, resistance, and mass per unit length. The resistance calculation takes into account the conductance values of the nanoribbon and junction. The model is validated using conduction calculations for undoped GNR junction cascades. The performance of the modeled nanowires, compared to copper, is presented in terms of specific conductivity. Different doping configurations and densities are considered, and it is found that doped GNR conductors can potentially outperform copper. However, the actual macroscale performance may be lower than the theoretical maximum due to factors such as the mass efficiency of nanowires, doping efficiency, and the need for larger fractional overlaps for mechanical strength. The comparison with experimental data for potassium-doped graphene sheets shows good agreement, but there is a lack of experimental data for iodine-doped graphene. Below is Figure 4.20 (a) and (b) which show the relative specific conductivity for potassium-doped GNR based on the fractional overlap of the nanoribbons θ. Figure 4.20(b) scrutinizes simulation versus experiment of non-ideal nanowires.

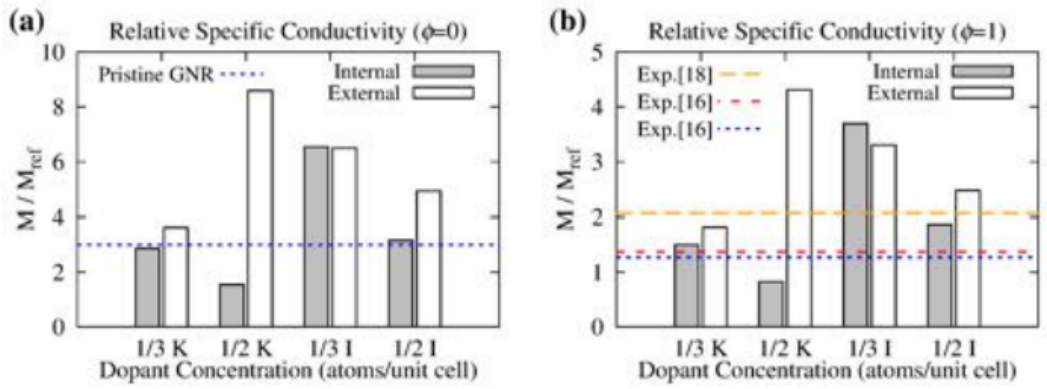

3.5 Chapter 5: Conductance of Curved 3M-1 Armchair Graphene Nanoribbons

3.5.1 Numerical Model

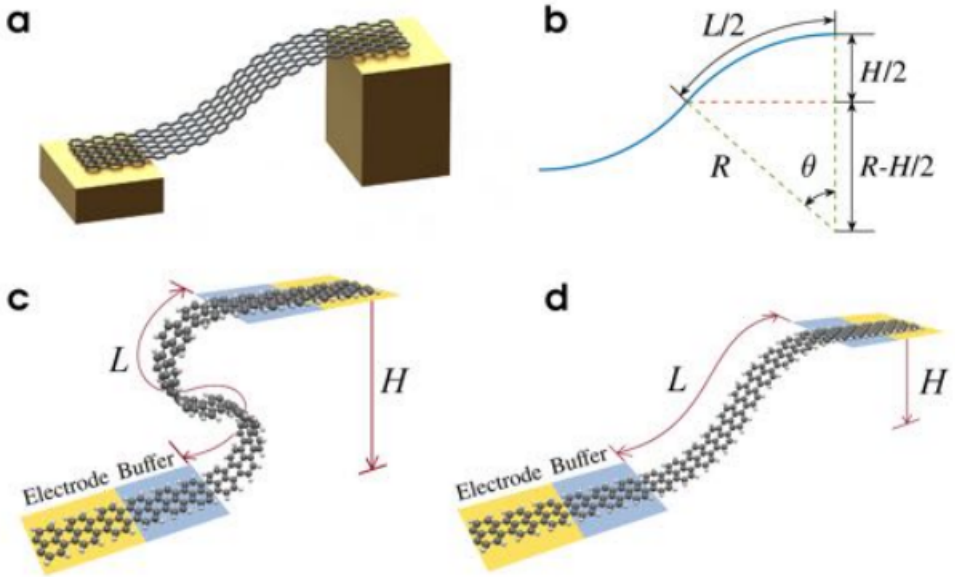

The section describes a generic nanoribbon model, which is illustrated in Figure 5.1 above. The model consists of a curved nanoribbon connected to two electrodes. The computational model is initialized using the geometry of the curved segment of the nanoribbon, which is composed of two circular arcs defined by a rotation angle (θ) and a radius of curvature (R). The ends of the nanoribbon have a vertical separation distance (H), and the slopes of the curved portions are zero at their endpoints. The length of the curved segment (L) and the other parameters (θ, R, and H) are related by certain constraints. The nanoribbon has two flat sections attached to each end: a mechanical buffer and a computational electrode. The bias applied to the nanoribbon is determined by the voltage difference between the electrodes. The length of the nanoribbon that carries the current is determined by the sum of the curved segment length (L) and half the length of the mechanical buffer (L_{buf}). In the equilibrium calculations, the positions of atoms in the electrode and buffer regions are fixed, while the atoms in the curved portion of the nanoribbon are free.

The modeled nanoribbons are a type called 3M-1 aGNRs, where M is an integer. They have a unit cell length of 0.4278 nm and are edge-terminated by hydrogen atoms. These nanoribbons have a small

band gap and are close to being metallic. The modeling results in the next section consider variations in geometric parameters within specific ranges.

In addition to the nanoribbon model, the chapter also presents a nanowire model. This model extends the well-known exponential decay model for current flow in flat semiconducting nanowires under a bias voltage. The goal is to describe the effects of length and curvature on the nanoribbon current using a separable, two-parameter formulation (Equation 5.4).

$$\alpha(\eta) \equiv \frac{I(\eta, S, V)}{I^{\text{flat}}(S, V)} \quad , \quad \eta \in \{\theta, H\}$$

The current is represented as a function of the curvature parameter (either H or θ), the applied bias voltage (V), and the current in a corresponding flat nanoribbon at the same length and bias voltage. The current in the flat nanoribbon is defined by an exponential decay expression, where $I_o(S_o, V)$ is a constant, k(V) is the voltage-dependent inverse decay length, and So is the maximum nanoribbon length without exponential decay.

3.5.2 Discussion and Results

The computational results discussed in this section provide valuable insights into the behavior of 5-aGNRs (5-armchair graphene nanoribbons). Firstly, the ab initio modeling results for flat 5-aGNRs align with the well-known exponential decay relation observed in semiconducting nanowires. This suggests that the modeling approach is accurate in describing the conductance of these nanoribbons.

The analysis then extends to curved 5-aGNRs, comparing their ab initio modeling results to a proposed separable form of equation 5.4.

This extension allows for a more comprehensive understanding of the conductance properties of curved nanowires, building upon the existing model for flat nanoribbons.

Moreover, the analysis of curved nanowires is applied to 5-aGNRs of different lengths, specifically 8-aGNRs and 11-aGNRs. The results demonstrate how the curvature affects the current response of these nanoribbons to bias voltages. The changes in conductance observed in the curved nanowires can be attributed to modifications in bandgaps and scattering properties caused by the deformation of the nanowire structure.

The discussion delves into the strain distributions within the modeled nanoribbons, which have been a focus of previous computational work. The strain distributions are found to be predominantly tensile at the edges and compressive in the interior of the nanoribbons. These strain effects play a significant role in the overall electron transmission and contribute to the changes in conductance due to variations in nanoribbon width and curvature.

To validate the developed model, a comparison is made with published experimental data from a nanoribbon "lifting" experiment. The analytical model, based on the separable form of equation 5.4, is represented below in Figure 5.6.

This confirms the applicability of the model in describing the conductance properties of curved nanoribbons and highlights its potential for practical applications.

Overall, the computational results presented in this section provide valuable insights into the conductance behavior of 5-aGNRs, both flat and curved. The findings expand our understanding of nanowire conductance, especially in the context of curved nanoribbons, and pave the way for potential applications in nanoelectronics and other related fields.

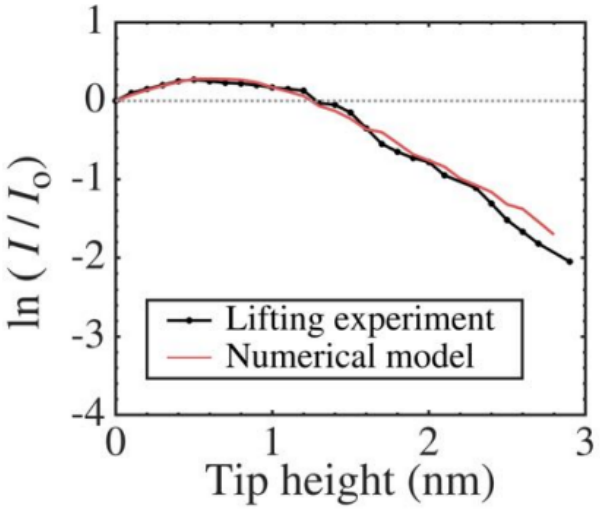

3.6 Chapter 6: Conductance of Buckled N=5 Armchair Graphene Nanoribbons

3.6.1 Numerical Model

The nanoribbons are hydrogen-terminated 5aGNRs (graphene nanoribbons) and are 16 unit cells long, with each unit cell measuring 0.428 nm. The nanoribbons are in equilibrium configurations at bulk strains of 0.61 and 0.74.

The modeled systems consist of two electrodes, two mechanical buffers, and a center section with an arc length denoted as L. The positions of atoms in the electrodes and mechanical buffers are fixed, while the atoms in the center section are initially positioned along four circular arcs of equal length, defined by a radius of curvature (R) and a rotation angle (θ). The slopes of the curves defining the atom positions in the center section are zero at the endpoints where the center section intersects the mechanical buffers. The horizontal separation distance between the mechanical buffers, referred to as the span (D), determines the bulk strain of the nanoribbon according to the equation

$$\epsilon = \frac{D}{L} - 1$$

The schematic in Figure 6.2(c) above illustrates the initial and equilibrium configurations of the buckled nanoribbons for various values of the initialization parameter (θ). It's important to note that for highly deformed nanoribbons, the initial and equilibrium configurations differ significantly, and the circular arcs parametrized by (θ) do not accurately describe the deformed shape. Therefore, another angular measure, total rotation (ϕ), is used to parametrize the equilibrium configurations. The total rotation (ϕ) is calculated by integrating the local rotation along the arc length of the center section, approximated by dividing the curved shape into straight line segments defined by nodal coordinates and summing the changes in rotation at the interior nodes.

$$\phi = \sum_{i=2}^{n-1} \left| \tan^{-1}\left(\frac{y_{i+1} - y_i}{x_{i+1} - x_i}\right) - \tan^{-1}\left(\frac{y_i - y_{i-1}}{x_i - x_{i-1}}\right) \right|$$

The total rotation (ϕ) is an extensive displacement variable that determines the effects of graphene nanoribbon curvature on conductance.

3.6.2 Results and Discussion

Previous research suggests that the current flow in semiconducting nanowires follows an exponential decay law and a similar form is assumed for flat semiconducting nanoribbons. The conductance model

accounts for the effects of curvature in highly deformed nanoribbons by introducing a function that represents the ratio of the current in a buckled nanoribbon to that of a flat nanoribbon. The effects of curvature are quantified by a state variable, which can be the bulk strain, the span, or the total rotation of the nanoribbon.

The current-voltage characteristics of different armchair graphene nanoribbons (AGNRs) are computed to evaluate the current ratio function. The results indicate that the total rotation of the nanoribbon plays a crucial role in determining the current flow. Local strain effects on conductance are found to be limited in buckled nanoribbons.

The passage also discusses the analytical description of the modeling results using fitted polynomials and a Lagrange interpolation. The functional forms and coefficients for the current ratio are provided for different nanoribbon lengths. The conductance model is compared to experimental data in Figure 6.6(a) below.

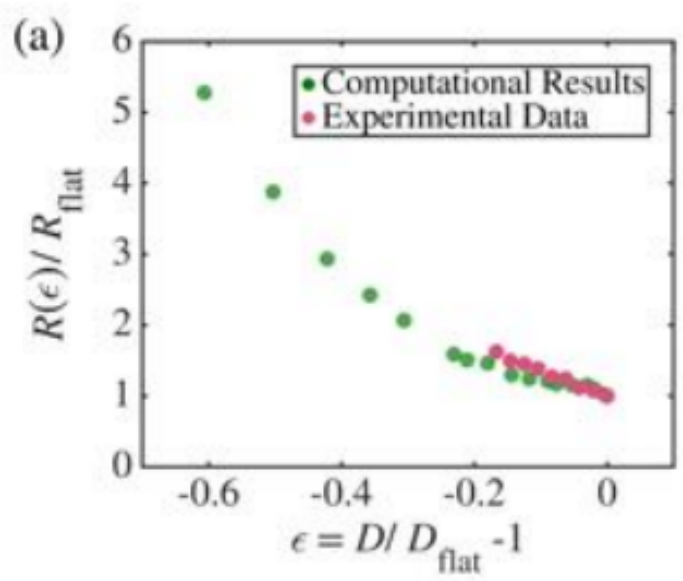

3.7 Chapter 7: Graphene Nanoribbons as Flexible Docks for Chemiresistive Sensing of Gas Phase Explosives

The chapter discusses the development of flexible sensors using graphene-based devices for gas phase sensing. Graphene-based sensors offer advantages like flexibility, high strength, electrical conductivity, thermal stability, and large surface area. The chapter explores various graphene configurations (pristine, functionalized, doped, nanoparticle-decorated, and nano-holed) for sensing gases such as carbon monoxide, nitrogen dioxide, ammonia, and explosives.

To overcome the challenges of chemiresistive sensing, the chapter proposes an adaptive sensor design using nanoelectromechanical systems (NEMS). Instead of specific ligands for target molecules, a flexible, semiconducting graphene nanoribbon (GNR) is used to adsorb the target molecule. The nanoribbon's shape is varied through mechanical actuation, and the resulting chemiresistive signature (current versus bias voltage and deformed shape) is compared with a database to identify the analyte. The chapter presents numerical models and results showing the response of the sensor to various analytes, including background gases and explosive molecules.

The proposed sensor offers advantages such as ease of fabrication, no chemical treatment requirement, selectivity, controllable actuation, and potential application to various target molecules. It can complement existing explosives detection methods and may find use in diverse applications.

3.8 Conclusion

This dissertation focused on graphene-based explosive sensors, investigating their sensing performance, conductance behavior, and adaptive design for gas phase explosives. The research explored various sensor parameters, including doping effects, junctions, bending, and docking methods. It introduced an adaptive ab initio molecular dynamics formulation and studied chemiresistive sensing of graphene-based sensors. The study demonstrated the potential of doped graphene nanoribbons as high-conductivity wiring and investigated conductance properties in curved nanoribbons. The dissertation proposed flexible graphene nanoribbons as docks for chemiresistive sensing, providing versatile and selective capabilities. Overall, the research advanced the field of nanocomposite explosive sensing systems, offering new insights and potential applications.